Precise β branching-ratio measurement for the 0^{+}→0^{+} superallowed decay of ^{34}Ar

V. E. Iacob, J. C. Hardy, H. I. Park, M. Bencomo, L. Chen, V. Horvat, N. Nica, B. T. Roeder, A. Saastamoinen, and I. S. Towner

Phys. Rev. C **101**, 045501 — Published 7 April 2020

DOI: 10.1103/PhysRevC.101.045501

Precise β branching-ratio measurement for the $0^+ \rightarrow 0^+$ superallowed decay of ^{34}Ar

V. E. Iacob,* J. C. Hardy,† H. I. Park, M. Bencomo, L. Chen, V. Horvat, N. Nica, B. T. Roeder, A. Saastamoinen, and I. S. Towner
Cyclotron Institute, Texas A&M University, College Station, Texas 77843-3366, USA
(Dated: January 22, 2020)

We have measured the branching ratio for the superallowed $0^+ \rightarrow 0^+$ β transition from ^{34}Ar to be 0.9448(8), and determined its ft value to be 3058.1(28) s, a result with $\pm 0.09\%$ precision, which is a factor of three improvement over the previous result based on current world data. The ft-value ratio for the mirror pair of superallowed transitions $^{34}\mathrm{Ar} \rightarrow ^{34}\mathrm{Cl}$ and $^{34}\mathrm{Cl} \rightarrow ^{34}\mathrm{S}$, becomes the most precise yet measured and, in a sensitive test of the method used to calculate the isospin-symmetry-breaking correction, δ_C, it agrees well with the ratio as calculated with Woods-Saxon radial wave functions. This confirms the method used in the most recent survey of superallowed decays to extract V_{ud}, the up-down quark-mixing element of the Cabibbo-Kobayashi-Maskawa matrix. In addition, our branching-ratio results for the four observed Gamow-Teller branches to 1^+ states in ^{34}Cl are shown to agree well with shell-model calculations based on the same effective interactions that were used in the determination of δ_C.

I. INTRODUCTION

Superallowed β-decay between $J^\pi = 0^+$, $T = 1$ analog states has long been used to probe the universality of the weak interaction. Currently, an ensemble of 14 such transitions is the source of the most precise value for V_{ud}, the up-down quark-mixing element of the Cabibbo-Kobayashi-Maskawa (CKM) matrix and a key ingredient in the most demanding test of that matrix's unitarity [1]. Uncertainties are all-important here since any deviation from unitarity would be a signal for new physics beyond the standard model. The ft values for these transitions have all been measured with high precision ($\pm$0.01-0.3%); their corrected $\mathcal{F}t$ values determined to be consistent with one another; and the implied value of V_{ud} established with $\pm 0.02\%$ precision.

As tiny as this uncertainty is, the experimental contribution to it is dwarfed by the contribution from theory. There are four small theoretical corrections – all of order 1% – that are required to convert ft into $\mathcal{F}t$, and then to extract V_{ud} from an average of all the $\mathcal{F}t$ values. Because these are by far the dominant contributors to the V_{ud} uncertainty, subsequent measurements of $0^+ \rightarrow 0^+$ decays can only contribute usefully to the test of CKM unitarity if they can improve the precision of the *theoretical* correction terms, for example by ruling out whole classes of models used to calculate the two sets of nuclear-structure-dependent correction terms (see Refs. [2, 3]).

The superallowed $0^+ \rightarrow 0^+$ β-decay branch from ^{34}Ar is one of the transitions already being used in the determination of V_{ud}. However, its contribution has been minimal since its $\pm 0.3\%$ uncertainty marked it as being the least precise of all 14 contributing transitions [1]. This is particularly unfortunate, since the ^{34}Ar superallowed decay also can play a critical role in distinguishing among the various models that have been used to calculate the structure-dependent correction terms required to convert a measured ft value into a corrected $\mathcal{F}t$ value. This is because it is one of the relatively few measured superallowed transitions that have a mirror decay partner; in this case, the mirror partner to the $^{34}\mathrm{Ar} \rightarrow ^{34}\mathrm{Cl}$ decay is $^{34}\mathrm{Cl} \rightarrow ^{34}\mathrm{S}$. It turns out that the ratio of ft values for such mirror pairs is a particularly sensitive test of the model used to calculate the structure-dependent corrections [2].

The ft value for the $^{34}\mathrm{Cl} \rightarrow ^{34}\mathrm{S}$ superallowed transition is known to $\pm 0.03\%$ but, with the experimental uncertainty for $^{34}\mathrm{Ar} \rightarrow ^{34}\mathrm{Cl}$ being 10 times worse, the ft ratio for the $A = 34$ mirror pair was of no use in this test of the corrections. We report here a measurement of the superallowed branching ratio for ^{34}Ar, which leads to a factor of three reduction in the corresponding ft-value uncertainty and produces an ft-value ratio that can now make a definitive choice among theoretical model options.

II. EXPERIMENT

We produced pure ^{34}Ar samples using a 30A-MeV ^{35}Cl beam from the K500 superconducting cyclotron at Texas A&M University to initiate the reaction $p(^{35}\mathrm{Cl}, 2n)^{34}\mathrm{Ar}$. The target was liquid-nitrogen-cooled hydrogen contained at 2.0-atm pressure in a thin-walled gas cell, which was located in the target chamber of the Momentum Achromat Recoil Spectrometer (MARS) [4]. The fully stripped reaction ejectiles were spatially separated in MARS by their charge-to-mass ratio, q/m, leaving a >99% pure ^{34}Ar beam to emerge from the focal-plane extraction slits. After exiting the vacuum system through a 51-μm-thick Kapton window, this beam then passed through a 0.3-mm-thick BC-404 scintillator and a stack of aluminum degraders, before finally stopping in the 76-μm-thick aluminized Mylar tape of a fast tape-transport system.

After the primary ^{35}Cl beam from the cyclotron had

* iacob@comp.tamu.edu
† hardy@comp.tamu.edu

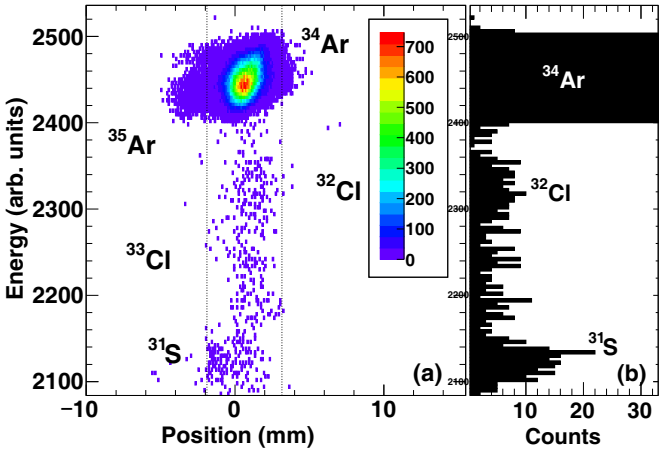

FIG. 1. (Color online) a) The deposited energy versus position as obtained with the PSSD in the MARS focal plane. The spectrometer had already been optimized for ^{34}Ar production and the extraction slits (vertical dotted lines) had been set. All the impurity-isotope labels are placed where the peaks of the respective activities had been seen with the slits wide open. b) The projection of total counts between the slits. From this and subsequent spectra recorded during our measurement, we established that the contribution of ^{32}Cl and ^{31}S to the extracted ^{34}Ar beam was 0.10(5)% and 0.43(14)%, respectively.

been fully tuned, we optimized the secondary ^{34}Ar beam purity through MARS before the measurement began. First, we inserted an attenuating grid into the cyclotron injection line to reduce the primary beam intensity, allowing us to place a 1-mm-thick 16-strip position-sensitive silicon detector (PSSD) at the MARS focal plane. Then, with the low-current primary beam, we focused the ^{34}Ar beam, identified nearby reaction products and minimized those that could affect the purity of the beam. With optimization completed and the focal-plane acceptance slits set, we obtained the result shown in Fig. 1. As is clear from the figure, there are only two residual impurities of any significance, ^{32}Cl and ^{31}S, both very weak: 0.10(5)% and 0.43(14)%, respectively, relative to ^{34}Ar. There are also some weak lighter-mass impurities cut off from the figure but they all have a much longer range than the ^{34}Ar, and pass entirely through the collection tape. None of these play any role in the measurement.

Following the optimization of MARS, the PSSD was removed from the beam path and the attenuating grid was withdrawn from the injection line, restoring the full primary beam intensity without any change in cyclotron or beam-line parameters. The measurement then began. We rechecked the composition of the beam daily during our measurement and again after it was completed by reinserting the attenuating grid and the PSSD, and recording the spectrum of deposited energy versus position each time. Small variations were observed and corrected from time to time; they were subsequently incorporated into our detailed off-line analysis.

Data-taking was in repetitive cycles. First, ^{34}Ar was collected in the tape for 2.0 s, its rate of accumulation being measured by the BC-404 scintillator located at the exit of MARS. Then the beam was interrupted at the cyclotron, and the tape-transport system was activated to move the sample in 230 ms to a shielded counting location 90 cm away, where decay data were acquired for 1.93 s. With counting completed, the beam was restored and the cycle repeated. To obtain adequate statistics, this clock-controlled sequence of collect-move-count was repeated over 70,000 times, with the results collected into nearly 120 separate "runs", averaging ∼600 cycles per run.

At the counting location were two detectors located on opposite sides of the tape. One, situated 3 mm away, was a 1-mm-thick BC-404 scintillator used to detect β^+ particles. Opposite it, at a nominal distance of 151 mm from the tape, was our high-purity germanium (HPGe) γ-ray detector, whose efficiency has been very precisely calibrated. The distance between the stopped tape and the HPGe detector was measured during the counting period of each cycle with a laser-ranging device [5] mounted next to the HPGe detector. The result, which was accurate to 30 μm, was recorded with the data for that cycle. The measured distances were quite consistent from cycle to cycle, with the full width at half maximum (FWHM) of their distribution being 0.4 mm, with a centroid at 151.17 mm. Because our HPGe-detector had been calibrated for efficiency at a source-detector distance of exactly 151.0 mm, we used the laser result to adjust the calibrated detector efficiency to correspond with the actual average source-detector distance. The difference being only 0.17 mm (0.1%), the adjustment was very small.

During the counting period of every cycle, our data-acquisition system generated a "master trigger" whenever a β particle and a γ ray were detected within ∼2 μs of one another. This signaled the occurrence of a β-γ coincident event and initiated acquisition. For each such event, we recorded the detected energy of both the β and γ rays, the precise time difference between their arrivals, and the time that the event itself occurred relative to the beginning of the counting period. For each cycle we also recorded the total number of β- and γ-ray singles, as well as the laser distance reading. The same discriminator signals used to scale the β singles were also used in creating the master triggers and establishing the occurrence of β-γ coincidences. Electronic dead times for the coincidence channel and the two singles channels were measured continuously throughout the measurement with pulser signals from a precise 1-MHz pulse generator being recorded in coincidence with the gating signals from each channel. Finally, we recorded with each cycle the rate of accumulation of ^{34}Ar ions in the tape as a function of time during the corresponding collection period.

We measured room background during the experiment to establish its contribution both to the β-γ coincidence spectrum and to the β-singles rate. To do this we used measurement cycles that were normal in every way except that the tape motion was disabled, so that the collected

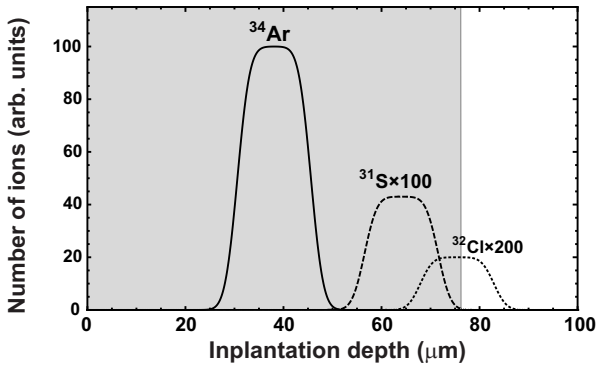

FIG. 2. Implantation profiles of ^{34}Ar (solid line) and the two contaminant activities ^{31}S and ^{32}Cl (dashed lines). The beam enters from the left. The shaded region shows the actual thickness of the Mylar collection tape. Our collected sample contains only those ions that are stopped in the tape.

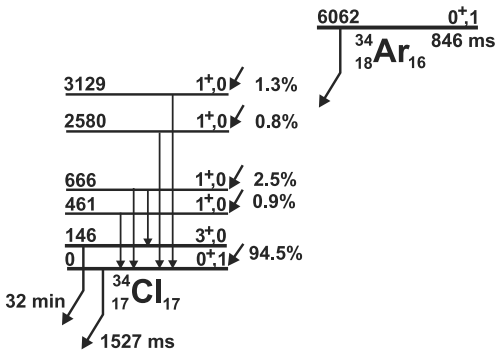

FIG. 3. Beta-decay scheme of ^{34}Ar, showing the five observed β-delayed γ-ray transitions in ^{34}Cl. Each energy level is labeled with its (J^π, T) as well as its energy, expressed in keV, relative to the ^{34}Cl ground state. Basic content is from the most recent evaluation [8]; however, the branching percentages and the presence of a γ-ray transition between the 666- and 146-keV levels come from this measurement.

sample never reached the counting location. Under these conditions, essentially no β-γ coincidences were observed, and the β-singles rate dropped to 0.012% of the rate observed under normal conditions. Though very low, this room-background rate for β-singles was incorporated into our analysis.

It is important to establish the role played by impurities in the collected samples. The two impurities identified in Fig. 1, ^{32}Cl and ^{31}S, have similar ranges to ^{34}Ar and, although weak, could be of concern. As in our previous published measurements (see, for example [6]), we obtained implantation profiles based both on calculations with the SRIM code [7] and on the depth distribution we determined for ^{34}Ar by measuring its collected activity as a function of degrader thickness. The result is given in Fig. 2 where the relative intensities have been chosen to reflect the measured PSSD intensities. Evidently all the ^{31}S ions stop in the tape and, with a half-life of 2.6 s, they must contribute to the β's detected during the counting period. As for ^{32}Cl, only half of it stops in the tape but, more importantly, it has a half-life of 298 ms: Most of it will have decayed away long before the count time begins. Ultimately, the samples present in the tape were 99.6% pure ^{34}Ar, with ^{31}S being the only perceptible impurity.

III. ANALYSIS

The β-decay scheme for ^{34}Ar is shown in Fig. 3. One branch is dominant: the strong superallowed transition that directly feeds the ground state of ^{34}Cl, which subsequently decays by another superallowed β transition to the ground state of ^{34}S. No γ rays whatsoever are emitted in this decay path. In contrast, all the allowed Gamow-Teller transitions from ^{34}Ar to excited 1^+ states are followed by prompt γ rays, predominantly emitted in each case directly to the ground state of ^{34}Cl.

It is these latter transitions whose absolute intensity we can measure from the β-coincident γ-ray spectrum. The total of the Gamow-Teller branching ratios can then be subtracted from 100% to yield the superallowed branching ratio. While the relative weakness of these transitions – they total only 5.5% – has a negative impact on the counting statistics that can be obtained in a measurement, it actually works to our advantage in another way. The percentage uncertainty on the measured Gamow-Teller intensity is reduced by a multiplicative factor of 0.06 (=5.5/94.5) when it is applied to the superallowed branch. A measurement precision of ±1.4% for the Gamow-Teller branches leads to a ±0.08% result for the superallowed branch.

To determine precisely the branching ratio for the superallowed transition from ^{34}Ar, our first step was to establish the β-branching ratio to the 666-keV 1^+ state in ^{34}Cl, the most intense branch observed. To do so, we determined the number of β-coincident 666-keV γ rays relative to the total number of positrons emitted from ^{34}Ar. Then, we used the relative intensities of all the other (weaker) observed γ-ray peaks to establish the total Gamow-Teller β-branching to all 1^+ states. Finally, the subtraction of this total from 100% resulted in the branching ratio for the superallowed transition.

To be more specific about our first step, we write the β^+-branching ratio, R_i, for a pure β^+-transition populating the particular state i, which is de-excited by the emission of a single γ ray, γ_i, as follows:

$$R_i = \frac{N_{\beta\gamma_i}}{N_\beta} \frac{\epsilon_\beta}{\epsilon_{\gamma_i}} \frac{}{\epsilon_{\beta_i}} , \qquad (1)$$

where $N_{\beta\gamma_i}$ is the total number of β-γ coincidences in the γ_i peak; N_β is the total number of beta singles corresponding to ^{34}Ar β decay; ϵ_{γ_i} is the efficiency of the HPGe detector for detecting γ_i rays; ϵ_{β_i} is the efficiency of the plastic scintillator for detecting the betas that populate state i; and ϵ_β is the average efficiency for detecting the betas from all ^{34}Ar transitions. Note that this equation only accounts for pure positron emission so, even

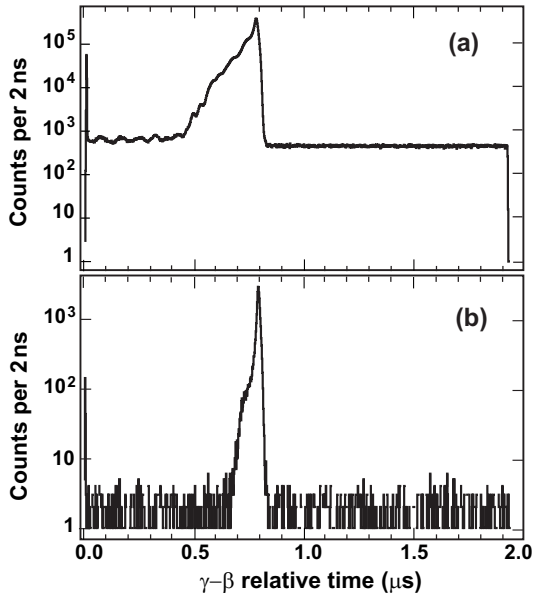

FIG. 4. (a) Spectrum of measured time-differences between the arrival of a γ ray and that of a β particle for all identified coincidence events. Note that the β signal was electronically delayed so that the prompt-coincidence peak appears near the center of the spectrum. (b) Measured time-difference spectrum for events corresponding only to the 666-keV γ ray.

though the contribution from electron capture for A=34 is very small, it must be separately accounted for. Furthermore, another small correction must be applied to incorporate the effect of the weak γ transition between the the 666- and 146-keV states in ^{34}Cl. Both these adjustments will be dealt with in Sec. IV.

In the immediately following sections, after describing some initial processing of the experimental data, we explain how all the factors on the right-hand side of Eq. (1) were obtained specifically for the β transition to the 666-keV state. Our approach is the same as the one we followed in previous measurements of the superallowed branching ratios from ^{26}Si [9] and ^{38}Ca [10] so we will be brief. The reader is referred to those earlier publications for more complete details.

A. Cycle selection

Before analysis began, we filtered our accumulated data by rejecting cycles that did not meet certain criteria. The first criterion we applied was the number of implanted ^{34}Ar ions detected by the BC-404 scintillator at the exit of MARS during each collection period. We rejected all cycles that had fewer than 1000 ions recorded, an indication of very little – or no – primary beam from the cyclotron. This removed ∼3% of the total cycles.

Our second criterion was based on the ratio of the number of β particles detected to the number of ^{34}Ar ions implanted for each cycle. We restricted this ratio for a given cycle to between 95 and 100% of the maximum value obtained for the whole run containing that cycle; this ensured that the tape-transport system had moved the ^{34}Ar sample into the designated counting position between the β detector and the HPGe detector. A serious deviation from this position could affect the effective efficiency of the HPGe detector for that cycle, so our selected limits were very conservative, and removed ∼34% of the cycles.

Our third criterion was a limit set on the reading from our laser measurement of the distance between the tape and the HPGe detector. We accepted cycles only if the distance was within ±0.34 mm of the central value. This removed only ∼3% of the remaining cycles.

In the end, our selection criteria provided 41,466 good cycles, ∼59% of the total cycles recorded. These good cycles contained approximately 1.4×10^7 β-γ coincidences, corresponding to over 5.8×10^8 β singles. All subsequent analysis incorporates only the data from these cycles.

B. Eliminating random coincidences

For each event, we recorded the time between the detection of a γ-ray and the subsequent arrival of an electronically delayed signal from the positron detector. The corresponding time spectrum for all identified events appears in the top panel of Fig. 4, in which the broad peak represents real (*i.e.* "prompt") coincident events, while the flat distributions to the left and right are from random coincidences. This time spectrum allowed us to produce a γ-ray spectrum free from random-coincidence events. We gated first on the part of the time spectrum that contains the prompt peak and then gated on the flat, random parts of the spectrum. The γ-ray spectrum

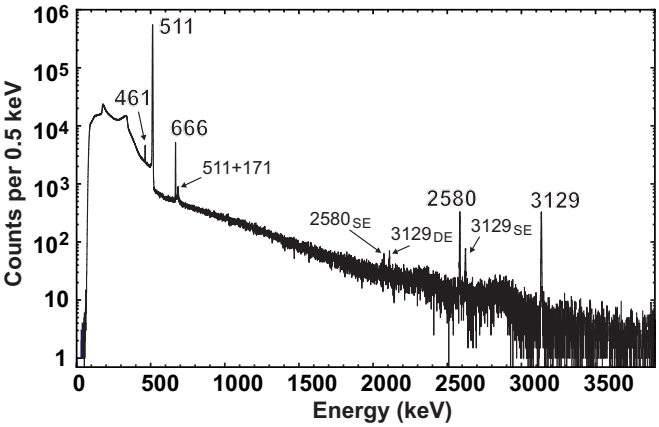

FIG. 5. Spectrum of γ rays observed in prompt coincidence with positrons from the decay of ^{34}Ar. The principal peaks are labeled with their energy in bold type and, where present, their corresponding single- and double-escape peaks are denoted by "SE" and "DE" subscripts, respectively. The small peak labeled "511+171" is due to the sum of two annihilation photons, one of which has backscattered into the detector.

obtained with the second gate, suitably normalized, was then subtracted from the spectrum obtained with the first gate. The result appears as Fig. 5. In addition to the annihilation radiation, the spectrum exhibits four clear full-energy γ-ray peaks from the decay of ^{34}Ar, at 461, 666, 2580 and 3129 keV, as well as escape peaks and a weak peak from coincident summing of two annihilation photons, one backscattered. No other peaks are immediately visible.

It is evident in the top panel of Fig. 4 that the prompt peak there has a noticeable tail to the left. This is because it incorporates all coincident events, covering a wide range of γ-ray energies. Low-energy γ rays trigger the TDC later than higher energy ones, and thus lead to a tail towards shorter times. The bottom panel of Fig. 4 shows the time spectrum corresponding to the single γ-ray peak at 666 keV. The prompt peak in this case is much narrower (FWHM <10 ns) and has only a weak tail. It is spectra like this, each restricted to a narrow energy window around a single γ-ray peak, that we used in our final analyses for the contents of individual peaks.

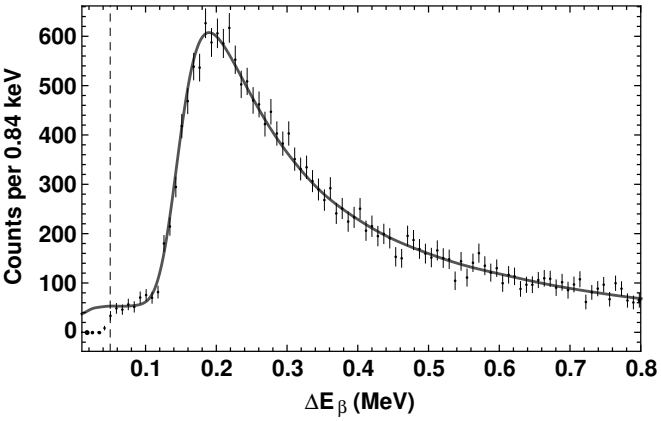

FIG. 6. The measured energy deposition (dots with error bars) in the β detector for the decay of ^{34}Ar to the 666-keV state in ^{34}Cl is compared with the EGSnrc-simulated spectrum (solid line). The dashed vertical line at 50 keV indicates our electronic threshold. The difference between the simulated and measured spectra below 50 keV indicates the events lost because of the threshold.

C. Efficiency calibrations

From Eq. (1) it is evident that our determination of the superallowed branching ratio relies critically on a precise absolute efficiency for the γ-ray detector, ϵ_{γ_i}, and equally precise relative efficiencies for the β detector, $\epsilon_\beta/\epsilon_{\beta_i}$.

Our HPGe detector has been meticulously calibrated at a source-to-detector distance of 151 mm. This was reported thoroughly more than a decade ago [11, 12]. Initially [11], we used 10 different radionuclides with accurately known relative photon emission rates together with two ^{60}Co sources specially prepared by the Physikalisch-Technische Bundesanstalt [13], having activities certified to $\pm$0.06%. The ^{60}Co sources were used to anchor our absolute efficiency calibration, with cascaded γ-ray transitions from the other sources providing precise links covering an energy range from 22 to 1836 keV.

We also made a number of measurements designed to reveal the physical dimensions and location of the detector's Ge crystal in its housing. This information was then used as input to Monte Carlo calculations performed with the electron and photon transport code CYLTRAN [14]. With only the thicknesses of the detector's two dead layers as adjustable parameters we achieved excellent agreement ($\chi^2/N = 0.8$) between the Monte Carlo efficiency results and our 40 measured data points. A year later, with three additional sources we extended our region of calibration up to 3.5 MeV [12].

Ever since these calibrations were made, we have kept the detector continuously at liquid-nitrogen temperature to ensure that the internal dead layer did not expand, and we have also periodically re-measured one of the precisely calibrated ^{60}Co sources. No change in detector efficiency has been detected, so we continue to use CYLTRAN calculations to obtain our detector efficiency with $\pm$0.2% uncertainty in the range 50-1400 keV, and with $\pm$0.4% from 1400 to 3500 keV.

The third column of Table I gives the efficiencies for the four main γ rays of interest as well as for a fifth weak γ ray at 519 keV, which will be discussed later.

Our β detector is a 1-mm-thick Bicron BC-404 scintillator disc optically coupled to a cylindrical Lucite light guide, which is coupled in turn to a photomultiplier tube. Its response function has been extensively characterized as a function of β-particle energy by a combination of GEANT4 [15] Monte Carlo simulations and measurements with ^{133}Ba, ^{137}Cs and ^{207}Bi sources, all three of which emit conversion electrons, and one, ^{137}Cs, emits β-decay electrons. The agreement between measurements and simulations was found to be excellent [16]. Since those studies were completed ten years ago, we have extended our source tests to ^{22}Na, with similar success; like ^{34}Ar, ^{22}Na is a positron emitter. We have also demonstrated that the EGSnrc Monte Carlo code [17] produces equally good agreement with measurements and runs faster than GEANT4, so we have used the former code in the present analysis.

As Eq. (1) makes clear, it is not the absolute efficiency of our β detector that is required, but rather how the efficiency changes as a function of the end-point energy, $E_{\beta max}$, which naturally is different for each β-decay branch feeding a state in ^{34}Cl. The energy dependence of our β-detection efficiency is caused principally by the fixed low-energy electronic threshold, which removes a slightly different fraction of the total β spectrum for different end-point energies. Since this affects the measured intensity of coincident γ rays following a β transition, it must be accurately accounted for even though the effect is very small.

Figure 6 presents the β-detector energy spectrum mea-

TABLE I. Detector efficiencies are given for the γ rays, γ_i, that de-excite states E_{x_i} in ^{34}Cl; and for β particles emitted in the decay branches, β_i, that populate states E_{x_i}. Calculated ratios of electron-capture to positron emission (ec/β^+) also appear for each decay branch. The values for ϵ_{γ_i} apply to our HPGe detector, and the ratios, $\epsilon_\beta/\epsilon_{\beta_i}$, to our thin β scintillator.

E_{x_i} [a] in ^{34}Cl (keV)	E_{γ_i} [a] for γ decay (keV)	ϵ_{γ_i} (%)	$E_{\beta max}$ for β_i feeding (keV)	$\epsilon_\beta/\epsilon_{\beta_i}$	ec/β^+
0.0	–	–	5039.9	0.9996	0.0007
461.0	461.0	0.4165(8)	4578.9	0.9993	0.0009
665.6	519.2	0.3801(8)	4374.3	0.9989	0.0010
665.6	665.6	0.3200(6)	4374.3	0.9989	0.0010
2580.4	2580.4	0.1179(5)	2459.5	1.0153	0.0058
3129.1	3129.1	0.0989(4)	1910.8	1.0266	0.0124

[a] Values taken from Ref. [8].

sured in coincidence with 666-keV γ rays. It singles out the β transition from ^{34}Ar feeding the 666-keV state in ^{34}Cl and is compared in the figure with a Monte-Carlo spectrum for the same transition, generated with EGSnrc. In the simulation we have included the transport tape, together with the rest of the nearby counting-location geometry. Clearly there is excellent agreement between the simulated and measured spectra above the electronic threshold, which gives us confidence that we can use the simulations to obtain reliable efficiency ratios, $\epsilon_\beta/\epsilon_{\beta_i}$, for the transitions of interest.

The fifth column of Table I lists our calculated results for the transitions of interest based on our electronic threshold being set at 50 keV. They appear without uncertainties since all are quite near unity and have uncertainties that are negligible in the present context. The calculated absolute β efficiency for the total of all decay branches from ^{34}Ar, ϵ_β, is approximately 45%. Its precise value is not required.

D. Beta singles

The N_β term in Eq. (1) refers to the total number of beta particles emitted in the decay of ^{34}Ar. The number we actually record from the β detector includes not only the β's from ^{34}Ar but also those from its daughter ^{34}Cl. In addition there are very weak contributions from β particles emitted in the decay of the ^{31}S impurity, and from γ rays in the ^{34}Ar decay chain registering in the β detector. We deal with these contributions individually.

1. Impurity

In Section II we established that the only impurity present in the tape during counting periods was ^{31}S; and determined it's average collection rate to be 0.43(14)% that of ^{34}Ar. Since ^{31}S decays ∼99% to the ground state of ^{31}P, its contribution to the β-coincident γ-ray spectrum of Fig. 5 would be negligible. Not so for the β-singles count, N_β. Taking account of the half-lives of ^{31}S, ^{34}Ar and ^{34}Cl, we calculate that the eventual contribution of ^{31}S to the total number of β particles recorded during the counting period must have been 0.18(6)%.

2. Gamma rays registering in the β detector

Gamma rays produced in the decay of ^{34}Ar have a very small probability of being counted in the β scintillator. For the strongest, 511-keV γ rays, this is irrelevant since annihilation radiation can be thought of as a surrogate for a β particle; in that case its presence would not alter the efficacy of Eq. (1). However it could be relevant for the transition γ rays in cases where they are detected but the corresponding β particle that feeds the transition is not. Using EGSnrc Monte Carlo simulations, we determined that 0.017(2)% of the total counts in the β detector are γ rays of this type. Although it has an essentially negligible effect, for completeness we reduced the recorded number of counts in the detector by this factor.

3. Parent β-decay fraction

Of much more significance is the contribution to the measured β singles from the decay of ^{34}Cl, the daughter of ^{34}Ar. This nuclide is not at all present in the implanted beam, but it naturally grows in the collected sample as ^{34}Ar decays. Fortunately, the half-lives of both parent and daughter are well known, ^{34}Ar being 846.46(35) ms [18] and ^{34}Cl, 1526.55(44) ms [1]. Consequently, the ratio of their activities can easily be calculated if the ^{34}Ar implantation rate is known as a function of time during the collection period. To enable this calculation, we recorded the arrival-time spectrum of ions detected by the scintillator at the exit of MARS for each individual cycle. A typical result for a single run appears as Fig. 7.

For us to extract the activity ratio for the singles events that we actually recorded in our β detector, two other factors must be considered. The first is our relative detection efficiency. Although the $E_{\beta max}$ for ^{34}Cl decay is less than it is for the superallowed transition from ^{34}Ar, the other lower-energy branches from ^{34}Ar act to offset the efficiency difference that would otherwise be expected (see discussion in Sec. III C). As a result, the total efficiency for observing β's from ^{34}Cl fortuitously turns out to be exactly the same as it is for observing them from ^{34}Ar.

The second factor to consider is the effect of the 519-keV γ-ray transition, which feeds the 32-minute isomeric state at 146-keV in ^{34}Cl, and thus steals a tiny amount, 0.036(5)%, of the ^{34}Ar strength away from the ^{34}Cl ground-state decay. In effect, this reduces the efficiency for detecting ^{34}Cl β's by the same amount.

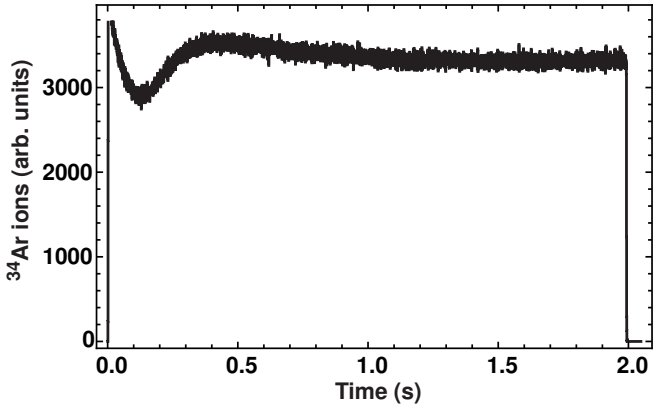

FIG. 7. Typical arrival-time spectrum of the collected ^{34}Ar ions measured over the course of one run. The initial drop in intensity is generated by the decrease in local density of the hydrogen in the target cell as the primary beam heats the gas around its path. A fan located inside the gas target mitigates the effect and ensures a rapid transition to stable conditions.

We are now in a position to calculate what fraction of the true A=34 β-decay events recorded in our detector is due to ^{34}Ar decay. Using the measured arrival-time spectrum of the ^{34}Ar ions (see Fig. 7), together with the known half-lives of ^{34}Ar and its daughter ^{34}Cl, we calculated the total number of decays of each, integrated over the precisely delineated counting period. The fraction attributable to ^{34}Ar was thus found to be 0.4636(2). This includes the effect of the 519-keV transition.

4. *Final result for N_β*

The steps required to obtain N_β appear quantitatively in Table II. Starting from the total counts recorded in our β detector, we first remove room background, and then correct for β-decay events from impurities and for γ rays counted in the β detector. Finally we apply the calculated ^{34}Ar β fraction. The final result for N_β appears on the bottom line of the table.

E. β-coincident 666-keV γ rays

The starting point for us to obtain $N_{\beta\gamma_{666}}$, the number of β-coincident 666-keV gamma rays, is the integrated area of the 666-keV γ-ray peak recorded in coincidence with the prompt peak in the γ-β time spectrum: See Fig. 4 and the description in Sec. III B. This peak area, like all others needed for this measurement, we determined using a modified version of GF3, the least-squares peak-fitting program in the RADWARE series [19]. A combined Gaussian and skewed Gaussian peak with a smoothed step function and a linear background in the peak region were sufficient to properly describe the detailed shape of all peaks of interest in the spectrum of Fig. 5. This was the same fitting procedure as was used in the original detector-efficiency calibration [11, 12]. The number of counts we obtained in this way for the 666-keV peak appears in the top row of Table III.

TABLE II. Derivation of N_β from the total number of singles events recorded in the β detector

Quantity	Value	Source
Total β-detector counts	$5.77359(24) \times 10^8$	
Background	$-6.803(26) \times 10^4$	Sec. II
β-decay of impurities	$-0.18(6)\%$	Sec. III D 1
Detected γ rays	$-0.017(2)\%$	Sec. III D 3
^{34}Ar fraction of β's	$\times 0.4636(2)$[a]	Sec. III D 3
$N_\beta(^{34}\mathrm{Ar})$	$2.6710(20) \times 10^8$	

[a] Calculation takes account of the weak 519-keV γ-decay branch from the 666-keV state to the isomeric state at 146 keV, which does not feed the superallowed decay of the ^{34}Cl ground state.

Before this result can be used in Eq. (1), there are several small corrections that must be applied to account for coincidence summing, dead-time and pile-up. These corrections are outlined in the following sections.

1. *Coincidence summing*

The 666-keV state in ^{34}Cl is fed by a positron decay branch from ^{34}Ar. For the γ ray from its subsequent decay to be recorded in our measurement, the positron must have appeared in our β detector in coincidence with the γ ray in our HPGe detector. Because the positron generally annihilates in or near the β detector, there is a non-negligible probability that one of the resulting 511-keV photons will also be recorded in the HPGe detector, and will sum with the 666-keV γ ray, thus removing some of the latter events from the full-energy peak. The resultant sum peak at 1177 keV (666 + 511) is too small to be visible in the β-coincident γ-ray spectrum shown in Fig. 5, but it is identifiable as a peak above background and we could determine its area, albeit with a rather large uncertainty.

The sum peak accounts only for a portion of the total events lost from the peak at 666 keV. To determine the total losses, we must incorporate the complete 511-keV response function, since losses from the 666-keV peak also result from summing with signals from 511-keV photons that Compton scatter in the HPGe crystal and deposit less than their full energy. This requires the ratio of the total efficiency of our detector to its full-energy-peak efficiency – the total-to-peak ratio – for 511-keV photons, a ratio we have already determined for our experimental conditions using a ^{68}Ge source [10]. After a small adjustment to incorporate the effects of annihilation in flight that apply specifically to ^{34}Ar decay, we determine the ratio to be 3.63(3).

This total-to-peak ratio multiplied by the area of the

TABLE III. Derivation of $N_{\beta\gamma_{666}}$ from the total number of events in the 666-keV peak in the β-coincident γ-ray spectrum.

Quantity	Value	Source
Area of 666-keV peak	20,224(171)	
511-keV summing	+581(145)	Sec. III E 1
bremsstrahlung summing	+0.21(3)%	Sec. III E 1
Dead time/pile-up	+1.43(10)%	Sec. III E 2
Random preemption	+0.35(2)%	Sec. III E 3
$N_{\beta\gamma_{666}}$	21,220(235)	

1177-keV sum peak establishes the total losses from the 666-keV peak due to summing with annihilation radiation to be 581(145) counts. This result appears as a correction to the 666-keV peak area in Table III.

External bremsstrahlung, emitted when positrons from ^{34}Ar slow down in the β detector or its surroundings, is another source of coincidence summing, but one that does not leave a characteristic sum peak. It results instead in a continuous energy spectrum indistinguishable from the summed Compton distributions resulting from detected γ rays. To arrive at the total contribution from bremsstrahlung in the spectrum of Fig. 5, we first took the areas of all γ-ray peaks, including the 511-keV peak, multiplied each by its corresponding total-to-peak ratio, summed the results and subtracted the sum from the total number of counts in the spectrum. We took this difference to be the contribution from bremsstrahlung. Combining this number with the full-energy-peak efficiency of our detector for 666-keV γ rays, we could calculate the probability for coincidence summing between those γ rays and the bremsstrahlung. We determined the resultant loss from the 666-keV peak to be 42(6) counts or 0.21(3)% of the total. This amount appears as a small applied correction in Table III.

An alternative approach is to determine the total coincidence summing – annihilation plus bremsstrahlung – in a single step. In this approach, only the true γ-ray peaks (*i.e.* excluding the annihilation radiation), multiplied by their respective total-to-peak ratios, are subtracted from the total number of counts in the coincident γ-ray spectrum. The difference, when divided by the area of the 511-keV peak, yields a redefined "total-to-peak" ratio for that peak, which now includes in the "total" the effects from annihilation in flight and bremsstrahlung, in addition to Compton scattering. Not surprisingly, this leads to a correction that is statistically consistent with the sum of the two correction terms – 511-keV summing, and bremsstrahlung summing – that are given individually in Table III.

2. Dead time and pile-up

Dead time in the β-detection system is only 450 ns per event, and since it affects both the numerator and denominator in Eq. (1) equally, there is no need to consider it any further. However, dead time and pile-up do affect the much slower signals from the HPGe detector, and their impact depends not only on the rate of coincident γ rays, which averaged 190 counts/s, but also on the singles γ rate, which averaged 685 counts/s. Furthermore, the rate during each cycle naturally decreased with time.

The dead time per event for encoded coincident γ rays was measured on-line to be 25.6 μs, a value that encompasses the pile-up time. For singles γ rays, which were not encoded, pile-up is the dominant effect, with its time determined from the signal pulse shape to be 17 μs per event. Since both dead time and pile-up remove legitimate signals, we treat them together. We calculated the total losses from both sources by integrating over the whole counting period, incorporating the decrease in rate caused by the decay of ^{34}Ar, and the growth-and-decay of ^{34}Cl. Our result, appearing in Table III, is that losses due to the combination of dead time and pile-up amount to 1.43(10)%.

3. Random preemption of real coincidences

There is a small probability that coincidences get lost as a result of a random coincidence preempting a real one. This can occur if a master trigger is generated by a real β-γ coincidence, which starts our timing clock (the TDC), but a random β event stops the clock before the true coincident β does. This effect can easily be calculated from the known rate of β signals and the time between the clock start and the appearance of the prompt peak: see Fig. 4(b). We calculated the loss from this effect to be 0.35(2)%, the amount shown in Table III.

4. Final result for $N_{\beta\gamma_{666}}$

All the corrections to the measured area of the 666-keV peak listed in Table III are additive, since they account for various identified losses. We first add back the counts lost to coincidence summing, then correct for losses due to dead time, pile-up and random preemption of true coincidence events. The resultant value for $N_{\beta\gamma_{666}}$ appears in the last row of the table. It is the last piece of input data required to complete the right-hand side of Eq. (1).

It has already been noted, though, that Eq. (1) only yields the β branching ratio under very restrictive conditions. In fact, in our case it yields the β-branching ratio for production of 666-keV γ rays. This is only equal to the β branching ratio to the 666-keV level if that state is solely populated by β decay and is de-populated by a single γ transition. This is almost, but not entirely, true. As described in the next section, there are other weak γ transitions that must be considered and, if necessary, accounted for before the true β branching ratio to this state, or any of the other 1^+ states, can be established.

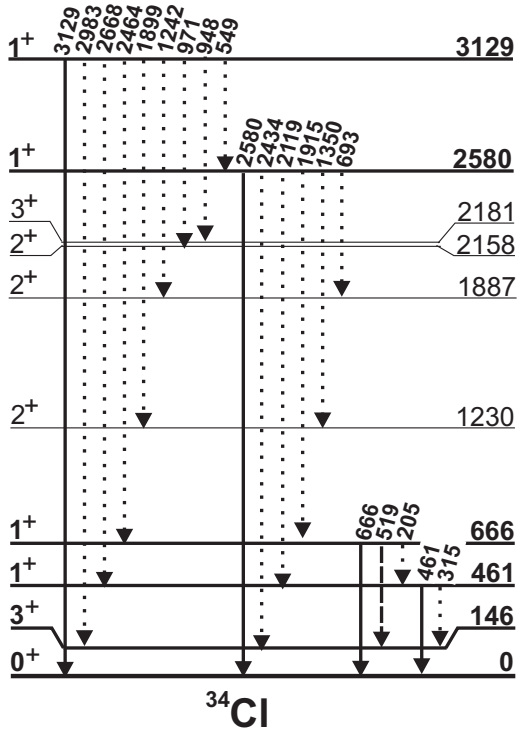

FIG. 8. Partial level scheme of ^{34}Cl, showing the excited states populated by the β decay of ^{34}Ar and the γ transitions that occur or may occur following the β decay. The four transitions shown with solid lines are the strongest ones; they correspond to the γ-ray peaks identified in Fig. 5. The weak 519-keV transition, shown dashed, is masked by the tail of the 511-keV peak in the spectrum in Fig. 5 but its strength has been determined. All five of these transitions appear in the decay scheme in Fig. 3. The dotted lines indicate possible weaker transitions, for which we set only upper limits.

F. Relative γ-ray intensities

In Fig. 5 we have identified four prominent γ-ray peaks from the decay of ^{34}Ar. The levels in the daughter, ^{34}Cl, are well known and, as illustrated in Fig. 3, the observed γ rays de-excite four 1^+ states directly to the ground state. These being the only 1^+ states known in this energy region [8], we would not anticipate the appearance of any other allowed Gamow-Teller β transitions, and forbidden transitions would be too weak to be relevant. However, the four states that are populated by allowed β decay do have other γ-decay options that are energetically available to them. These are explicitly identified in Fig. 8.

The energy response of our HPGe detector was determined before our experiment began with a ^{152}Eu calibration source, and reinforced by the well known energies of the four principal γ rays observed during the experiment. With this calibration, we searched carefully in our data for γ-ray peaks corresponding to any of the potential transitions presented in Fig. 8, but only one could be identified: the 519-keV peak corresponding to the transition between the 666- and 146-keV levels. For all other potential transitions, we have set upper limits on their intensity.

TABLE IV. Relative intensities of β-delayed γ rays from the β^+ decay of ^{34}Ar.

	I_γ			
E_γ [keV]	Ref. [20]	Ref. [21]	This work	Adopted
205		<0.010	<0.013	<0.010
315		<0.0018	<0.0086	<0.0018
461	0.365(36)		0.353(9)	0.354(9)
519		<0.010	0.029(10)	0.0146(19)[a]
549			<0.0045	<0.0045
666	1	1	1	1
693		<0.010	<0.0026	<0.0026
948		<0.015	<0.0033	<0.0033
971		<0.015	<0.0034	<0.0034
1242		<0.010	<0.0056	<0.0056
1350		<0.0034	<0.0041	<0.0034
1899		<0.010	<0.0055	<0.0055
1915		<0.0068	<0.0032	<0.0032
2119		<0.0068	<0.0035	<0.0035
2434		<0.0068	<0.0026	<0.0026
2464		<0.015	<0.0027	<0.0027
2580	0.345(10)		0.338(8)	0.341(6)
2668		<0.010	<0.0029	<0.0029
2983		<0.010	<0.0022	<0.0022
3129	0.521(12)		0.511(10)	0.515(8)

[a]Result taken from Ref. [23].

The relative intensities and limits we obtained for all the β-delayed γ-rays observed in the decay of ^{34}Ar are listed in the fourth column of Table IV. In determining each γ-ray intensity in the table, we have incorporated the β-detector efficiency given in column 5 of Table I for the β transition that populates the state from which each originates. Furthermore, since we recorded only β-coincident γ rays, we have also corrected the relative intensities to include the small calculated contributions from electron-capture decay (see column 6 of Table I).

The 519-keV transition plays a critical role in our determination of the β-decay branching to the 666-keV level since it participates directly in the de-excitation of that level. Unfortunately, the area of the 519-keV γ-ray peak is difficult to quantify precisely in our data since it lies in the tail of the strongly dominant 511-keV annihilation peak, as can be seen in Fig. 9. This severely limits the precision of the relative intensity value we quote for the 519-keV γ ray under "this work" in Table IV.

In addition to our results, Table IV includes results from the only previous ^{34}Ar β-decay measurement with useful precision [20], together with limits derived principally from (p,γ) results as summarized by Endt in Table 34.17 of Ref. [21]. Our results are more precise than, but agree well with, the previous measurement of the principal γ rays; while our limits are generally tighter than the previous ones for all unobserved transitions. The

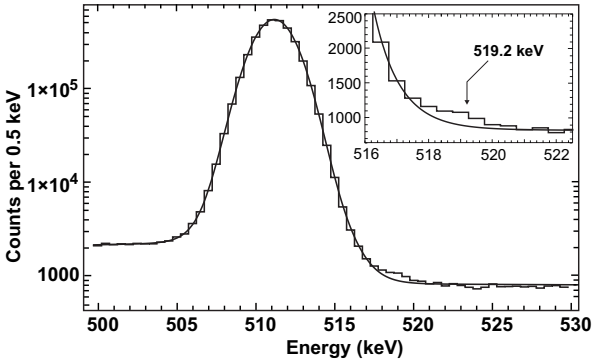

FIG. 9. Portion of the summed β-coincident γ-ray spectrum of Fig. 5, which focuses on the 511-keV annihilation peak and the weak 519-keV peak from the transition between the 666- and 146-keV states in ^{34}Cl. The inset focuses further onto the 519-keV peak. The histogram represents the data, while the smooth curve is the function we used to fit the 511-keV peak shape.

"adopted" values in the last column of Table IV are either an average of measured quantities, or the lower of the two limits where only limits have been determined. Note that there is one slight disagreement with a previous result: the intensity we measured for the all-important 519-keV peak is well above the upper limit previously quoted in Ref. [21] though, as it happens, it is somewhat below an earlier measurement [22] apparently rejected by Endt [21].

This discrepancy and the importance of the 519-keV peak intensity to our analysis led us to measure, in a different collaboration, the decay of the 666-keV state in ^{34}Cl, which was produced in the ^{33}S$(p,\gamma)^{34}$Cl reaction. The intensity ratio of the 519- and 666-keV peaks obtained in this measurement [23] is more than an order-of-magnitude more precise than any previous result so we adopt it unmodified in the fifth column of Table IV.

IV. RESULTS

A. Gamow-Teller branching ratios

In Sections III C, III D and III E we have obtained values for all the quantities on the right-hand side of Eq. (1). Using these results we determine that

$$R'_{666} = 0.02480(28), \tag{2}$$

where we adopt the prime on R to signify that R'_{666} refers only to the probability for producing a 666-keV γ ray from the β decay of ^{34}Ar. As illustrated in Fig. 8, the 666-keV state has two measured γ-ray branches, at 519 and 666 keV, and has a third 205-keV option, on the intensity of which we have set an upper limit. The state also can be fed, in principle, by γ-ray transitions of 1915 and 2464 keV; for those too we have upper limits on their intensities. All relevant quantities appear in Table IV. Taking account of all these values and limits, and continuing to use the same normalization as that used in the table, we determine the total relative β^+ feeding to the 666-keV level to be $1.015(^{+10}_{-5})$.

One last requirement is to take account of electron-capture feeding of the 666-keV state. Recognizing that both the numerator and denominator in Eq. (1) need to be corrected for missing electron-capture decays, we multiply the result for R'_{666} by $(1+\xi_{666})/(1+\xi)$, where ξ_{666} is the electron-capture-to-positron ratio (ec/β^+) for the β transition populating the 666-keV state and ξ is that ratio for the total decay of ^{34}Ar. The ec/β^+ ratios for all the transitions of interest appear in column 6 of Table I and yield the value $(1+\xi_{666})/(1+\xi) = 1.00104/1.00089)$ $= 1.00015$. This correction is negligible in the present context but is incorporated for completeness. The total relative (β^+ + ec) feeding to the 666-keV level is $1.015(^{+10}_{-5})$. This result appears in the third row, third column of Table V.

The final branching ratio for the (β^++ ec) transition to the 666-keV state is the product of R'_{666}, from Eq. (2), with the relative (β^+ + ec) feeding value just derived. The result is

$$R_{666} = 0.02517(^{+38}_{-30}), \tag{3}$$

which also appears in the third row, fourth column of Table V.

The branching ratios for the Gamow-Teller transitions to other levels in ^{34}Ar can be derived in the same way from the intensities of the γ rays that populate and depopulate those levels. The results appear in column three of Table V, where we have maintained the same normalization to the intensity of the 666-keV γ ray as in Table IV, and made use of Fig. 8, which shows the placement in the decay scheme of all the observed γ rays. After multiplying by the value for R'_{666} in Eq. (2), we arrive at the final branching ratios for the three remaining Gamow-Teller transitions from ^{34}Ar, which are listed in the fourth column of the table.

The derived log ft values for these transitions are given in column five of the table. To obtain them we used the energies, $E_{\beta max}$, from the second column of the table, combined with the ^{34}Ar half-life of 846.46(35) ms [18].

TABLE V. Measured β-branching ratios to all the states in ^{34}Cl populated by the β decay of ^{34}Ar.

E_{x_i}	$E_{\beta max}$	(β^++ ec) branching		
(keV)	(keV)	Relative	absolute	log ft
0	5039.9		0.9448(8)	3.4855(4)
461.0	4578.9	$0.354(^{+9}_{-14})$	$0.0088(^{+2}_{-4})$	$5.324(^{+20}_{-10})$
665.6	4374.3	$1.015(^{+10}_{-5})$	$0.0252(^{+4}_{-3})$	$4.776(^{+5}_{-7})$
2580.4	2459.5	$0.341(^{+9}_{-8})$	$0.0085(^{+3}_{-2})$	$4.122(^{+11}_{-16})$
3129.1	1910.8	$0.515(^{+14}_{-8})$	$0.0128(^{+4}_{-2})$	$3.466(^{+7}_{-14})$

TABLE VI. Uncertainty budget for ^{34}Ar branching ratios

Source	Uncertainty (%)	
	$\sum$GT branches	$0^+ \to 0^+$ branch
Counting statistics		
γ_{666} & β singles	1.10	0.065
$\sum\gamma/\gamma_{666}$	0.76	0.044
HPGe detector efficiency	0.20	0.011
Dead time	0.09	0.005
Contaminant contribution to β singles	0.05	0.003
^{34}Ar component of β singles	0.04	0.002
Bremsstrahlung coincidence summing	0.04	0.002
Peak-to-total ratio for 511-keV γ's	0.02	0.001
Random preemption of real coincidences	0.02	0.001
Total uncertainty	1.36	0.080

These data were used as input to the log ft calculator available at the National Nuclear Data Center (NNDC) [24] web site. The results obtained appear in the fifth column of Table V. They range from 3.5 to 5.3, which is well within the range that characterizes allowed $0^+ \to 1^+$ transitions [25].

B. Branching ratio for the superallowed transition

Summing the relative branching ratios in column three of Table V for the four Gamow-Teller transitions, we obtain $2.225(^{+21}_{-19})$. This result multiplied by R'_{666} from Eq. (2) yields 0.0552(8) the total absolute $(\beta^+ + \mathrm{ec})$ branching ratio to the 1^+ states in ^{34}Cl.

Before proceeding, it is important to be sure that there is not a large number of unobserved weak transitions to higher excited states that could sum to appreciable missed strength: the Pandemonium effect [26, 27]. Shell-model calculations to be described in Sec. V B, which show excellent agreement with the observed transition intensities, limit possible unobserved intensity feeding higher excited states in ^{34}Cl to being less than 50 parts per million, more than an order-of-magnitude less than our quoted uncertainty. We can safely conclude that the Gamow-Teller sum we have obtained accounts for all the non-superallowed strength in the decay of ^{34}Ar.

The branching ratio for the superallowed $0^+ \to 0^+$ transition to the ground state is thus 0.9448(8), a result we obtain simply by subtracting the total Gamow-Teller $(\beta^+ + \mathrm{ec})$ branching ratio, quoted above, from unity. This value, which has a precision of $\pm 0.08\%$ appears in the top line of the fourth column of Table V. The log ft value for the transition appears next to it in column five. In this case, where the greatest precision is required, we used the full calculation for the statistical rate function, f, as given in Ref. [1].

C. Uncertainty budget

A detailed uncertainty budget for our ^{34}Ar branching-ratio measurement appears in Table VI, where we present two relative uncertainties (in percent) for each contribution. The first is expressed relative to the total intensity of all Gamow-Teller branches; this is the uncertainty associated with the measurement itself. The second is expressed relative to the superallowed branching ratio, which is the derived quantity of principal interest.

Evidently, counting statistics are by far the largest contributors to the total uncertainty. The 666-keV γ ray, the strongest one we observe, follows a 2.5% Gamow-Teller β-decay branch from ^{34}Ar. Its intensity is thus 160 times less than that of the 511-keV positron-annihilation photons, which arise from all decay branches of both ^{34}Ar and its daughter ^{34}Cl. We have to limit our counting rate so as to keep dead-time and other corrections to a manageable size, but it is the annihilation rate that determines the limit. The relatively large counting-statistical uncertainties reflect the relatively few 666-keV γ-ray events that could be accumulated in a week-long measurement.

All the remaining contributions can be classified as systematic uncertainties. Altogether their contribution to the total is barely perceptible.

V. DISCUSSION

A. Superallowed decay branch

The branching ratios for the $(\beta^+ + \mathrm{ec})$ transitions from ^{34}Ar have been measured only once before, 45 years ago [20]. Remarkably, those earlier results agree completely with our new, more precise ones, as can be seen from the detailed comparison in Table VII. Since a weighted average of the two measurements of the superallowed transition is essentially the same as our new result, in the following development we will simply use the latter.

There have been no new measurements of the Q_{EC} value for the superallowed β branch from ^{34}Ar, so we adopt the f value, 3410.97(61) given for it in the most

TABLE VII. Comparison of our measured $(\beta^+ + \mathrm{ec})$ branching ratios from ^{34}Ar with the only previous measurement.

E_{x_i}	$(\beta^+ + \mathrm{ec})$ branching	
(keV)	Ref. [20]	this work
0	$0.9444(^{+23}_{-26})$	0.9448(8)
461.0	0.0091(10)	$0.0088(^{+2}_{-4})$
665.6	$0.0249(^{+13}_{-10})$	$0.0252(^{+4}_{-3})$
2580.4	$0.0086(^{+10}_{-4})$	$0.0085(^{+3}_{-2})$
3129.1	$0.0130(^{+12}_{-6})$	$0.0128(^{+4}_{-2})$

recent survey of superallowed $0^+ \rightarrow 0^+$ nuclear β decays [1]. However, there has been a new half-life measurement [18], which replaces the previously dominant one. We use the new value, 846.46(35) ms. In combination with our new branching-ratio measurement, these results yield

$$ft = 3058.1(28)\, s. \quad (4)$$

The relationship between an ft value and the $\mathcal{F}t$ value used to extract V_{ud} is given by

$$\mathcal{F}t \equiv ft(1+\delta'_R)(1+\delta_{NS}-\delta_C), \quad (5)$$

where δ_C is the isospin-symmetry-breaking correction and the terms δ'_R and δ_{NS} comprise the transition-dependent part of the radiative correction, the former being a function only of the decay energy and the atomic number Z of the daughter nucleus, while the latter, like δ_C, depends in its evaluation on the details of nuclear structure. Taking the values for these three small correction terms from Table IX in Ref. [1], we obtain the result,

$$\mathcal{F}t = 3074.0(34)\, s. \quad (6)$$

With 0.11% precision, this result for ^{34}Ar is competitive with $\mathcal{F}t$ values for the previously best-known $T_Z = 0$ superallowed emitters, all of which have branching ratios that are greater than 99.97% and thus did not require such a challenging measurement. Our new $\mathcal{F}t$ value for ^{34}Ar decay is entirely consistent with 3072.27(62) s, the average $\mathcal{F}t$ value quoted in Ref. [1] for all fourteen superallowed emitters well known at the time.

What makes the new ft value for the ^{34}Ar superallowed decay particularly interesting is the fact that it becomes one half of what is now the most precisely known mirror pair of superallowed transitions: *viz.* $^{34}\mathrm{Ar} \rightarrow {}^{34}\mathrm{Cl}$ and $^{34}\mathrm{Cl} \rightarrow {}^{34}\mathrm{S}$. If the constancy of $\mathcal{F}t$ is taken as a premise, then the ratio of ft values from a mirror pair relates directly to the calculated correction terms δ'_R, δ_{NS} and δ_C through the following equation:

$$\frac{ft^a}{ft^b} = 1 + (\delta'^b_R - \delta'^a_R) + (\delta^b_{NS} - \delta^a_{NS}) - (\delta^b_C - \delta^a_C)\ , \quad (7)$$

where, in the present case, superscript "a" denotes the decay $^{34}\mathrm{Ar} \rightarrow {}^{34}\mathrm{Cl}$ and "b" denotes $^{34}\mathrm{Cl} \rightarrow {}^{34}\mathrm{S}$. As explained in Ref. [3], the crucial advantage offered by Eq. (7) is that the theoretical uncertainty on a difference term such as $(\delta^b_C - \delta^a_C)$ is significantly less than the uncertainties on δ^b_C and δ^a_C individually. This means that the experimental ft-value ratio can provide a sensitive and independent test of the veracity of the correction terms, particularly δ_C.

Taking ft^a from Eq. 4, and ft^b from the most recent review of superallowed $0^+ \rightarrow 0^+$ decays [1], we determine the ratio for the $A = 34$ pair to be $ft^a/ft^b = 1.0028(10)$. This value agrees with 1.0017(3), the ratio obtained if Woods-Saxon radial wave functions are used to calculate the δ_C values, and disagrees significantly with the ratio 0.9997(4) calculated if Hartree-Fock radial wave functions [3] are used.

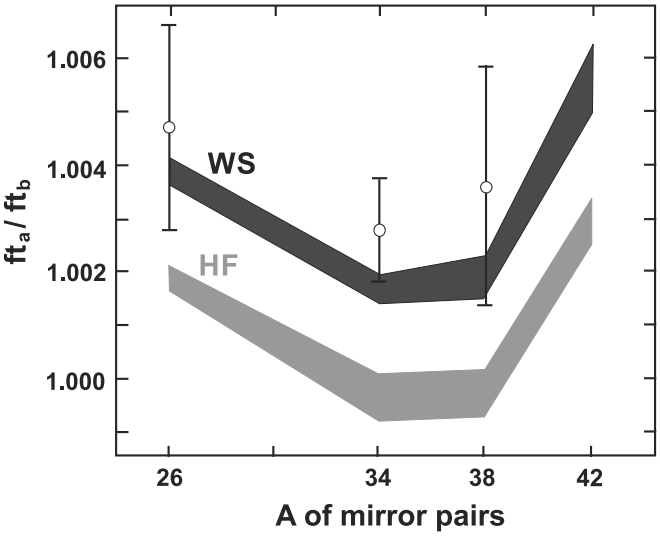

FIG. 10. Mirror-pair ft^a/ft^b values for A = 26, 34, 38 and 42, where the "a" and "b" superscripts denote decays of the T_Z = -1 and T_Z = 0 parents, respectively. The black and grey bands connect calculated results that utilize Woods-Saxon (WS) and Hartree-Fock (HF) radial wave functions, respectively. The measured results for A = 26, 34 and 38 appear as open circles with error bars.

The measured ratios for all three known mirror pairs—the present $A = 34$ result, together with the previously published results for $A = 26$ [9] and $A = 42$ [10]—are compared with calculated values [3] in Fig. 10. Taken collectively, the data are seen to strongly favor the Woods-Saxon-based calculations; quantitatively, the normalized χ^2 for the Woods-Saxon comparison is 0.84 (Confidence level, CL = 43%) and that for the Hartree-Fock is 6.22 (CL = 0.20%). This is a definitive selection between the two.

B. Gamow-Teller branches

From the nuclear-model perspective, both ^{34}Ar and ^{34}Cl are well described by *sd* shell orbitals. In Table VIII we show the results of *sd* shell-model calculations for 1^+ states in ^{34}Cl, involving the full *sd* shell with USD effective interaction of Wildenthal [28] and two more recent updates, USD-A and USD-B, of Brown and Richter [29]. In all cases we use a quenched value for the axial-vector coupling constant, $g_{A,\mathrm{eff}} = 1.0$, which Brown and Wildenthal [30] demonstrated to be appropriate for use in calculations truncated to just *sd*-shell configurations.

These calculations identify eight 1^+, $T = 0$ states in ^{34}Cl below the 6062-keV Q_{EC} value for ^{34}Ar decay [1]. The calculated energies and β-decay branching ratios are compared with experiment in Table VIII, from which it

TABLE VIII. Experimental and theoretical excitation energies and β-decay branching ratios, R, to the daughter 1^+ states in ^{34}Cl. The theoretical values were obtained from an *sd* shell-model calculation with effective interactions USD, USD-A and USD-B.

	Expt		USD		USD-A		USD-B	
State	E_x(keV)	R(%)	E_x(keV)	R(%)	E_x(keV)	R(%)	E_x(keV)	R(%)
$1^+_1, T=0$	461	0.88	320	0.28	550	0.47	330	0.26
$1^+_2, T=0$	666	2.52	660	2.24	270	2.09	520	6.42
$1^+_3, T=0$	2580	0.85	2520	0.69	2260	0.92	2370	0.28
$1^+_4, T=0$	3129	1.28	3250	0.85	3150	0.93	3050	0.90
$1^+_5, T=0$			3880	0.0003	3690	0.0028	3730	0.0010
$1^+_6, T=0$			3950	0.0017	4060	0.0022	3800	0.0015
$1^+_7, T=0$			4980	0.0008	4830	0.0015	4880	0.0008
$1^+_8, T=0$			5110	0.0005	5170	0.0000	5020	0.0006

is evident that there is very good correspondence between experiment and theory for the four lowest-energy 1^+ states, whose branching ratios have been measured. Overall, the USD effective interaction gives the closest match to the experimental results, but the other two interactions show acceptable agreement.

For precise β-decay studies such as the one reported here, it is essential to ensure that no decay strength remains unaccounted for. In particular, one must rule out – or correct for – low-energy β transitions to highly excited states, transitions that could be too weak to be observed individually but are numerous enough that their total intensity is of significance [26, 27]. As seen in Table VIII, our calculations predict four more 1^+ states at excitation energies above the four we have observed. The total predicted feeding of these states differs slightly from calculation to calculation, but is never higher than 65 ppm. Even this is an overestimate. Not all that strength would have been missed in our β-decay measurement, since some of the de-excitation γ-ray intensity feeds one of the four lower-lying 1^+ states. By also calculating the γ-ray de-excitation of these states, we determined that missed strength would actually be less than 50 ppm. This has negligible impact on our measurement.

VI. CONCLUSIONS

We report a precise measurement of the branching ratio for the superallowed $0^+ \rightarrow 0^+$ β decay of ^{34}Ar. It is not the first measurement of this quantity but its precision is a significant improvement over the only previous measurement. As a result, the corresponding improvements in the ft and $\mathcal{F}t$ values for this transition promote it to prominence among the most precisely known transitions of its type. The most powerful outcome is that the $A = 34$ mirror pair of $0^+ \rightarrow 0^+$ superallowed transitions, $^{34}\mathrm{Ar} \rightarrow ^{34}\mathrm{Cl}$ and $^{34}\mathrm{Cl} \rightarrow ^{34}\mathrm{S}$, becomes the most precisely characterized mirror pair, with its ratio of ft values providing key confirmation for the use of Woods-Saxon wave functions in calculations of the isospin-symmetry-breaking correction δ_C.

Not only is the superallowed branching-ratio measurement valuable, but also there is good agreement between our results and shell-model calculations for the Gamow-Teller decay branches to 1^+ states in ^{34}Cl. This is an important result since the same effective interactions were used in the shell-model contributions to the calculation of both δ_C and δ_{NS}. Our results demonstrate their efficacy for these nuclei.

The currently accepted value of V_{ud}, the up-down quark-mixing element of the CKM matrix, is determined from the average $\mathcal{F}t$ value for fourteen $0^+ \rightarrow 0^+$ superallowed transitions [1]; and each individual $\mathcal{F}t$ value that contributes to the average depends critically on its calculated δ_C and δ_{NS} correction terms. The correction terms used in the most recent survey [1] used the shell model to determine configuration mixing and Woods-Saxon radial wave functions to evaluate the radial mismatch between parent and daughter states. Our results for ^{34}Ar decay convincingly support these methods for calculating the structure-dependent correction terms.

ACKNOWLEDGMENTS

This material is based upon work supported by the U.S. Department of Energy, Office of Science, Office of Nuclear Physics, under Award Number DE-FG03-93ER40773, and by the Welch Foundation under Grant No. A-1397.

[1] J. C. Hardy and I. S. Towner, Phys. Rev. C **91**, 025501 (2015).

[2] I. S. Towner and J. C. Hardy, Phys. Rev. C **82**, 065501

(2010).
[3] H. I. Park, J. C. Hardy, V. E. Iacob, M. Bencomo, L. Chen, V. Horvat, N. Nica, B. T. Roeder, E. Simmons, R. E. Tribble and I. S. Towner, Phys. Rev. Lett. **112**, 102502 (2014).
[4] R. E. Tribble, A. Azhari, C. A. Gagliardi, J. C. Hardy, A. Mukhamedzhanov, X. Tang, L. Trache, and S. J. Yennello, Nucl. Phys. A **701**, 278 (2002).
[5] Acuity AR700-4 Laser Displacement Sensor, www.acuitylaser.com.
[6] V. E. Iacob, J. C. Hardy, L. Chen, V. Horvat, M. Bencomo, N. Nica, H. I. Park, B. T. Roeder and A. Saastamoinen, Phys. Rev. C **97**, 035501 (2018).
[7] J. F. Ziegler, www.srim.org/.
[8] N. Nica and B. Singh, Nuclear Data Sheets **113**, 1563 (2012).
[9] M. Bencomo, J. C. Hardy, V. E. Iacob, H. I. Park, L. Chen, V. Horvat, N. Nica, B. T. Roeder, A. Saastamoinen and I. S. Towner, Phys. Rev. C **100**, 015503 (2019).
[10] H. I. Park, J. C. Hardy, V. E. Iacob, M. Bencomo, L. Chen, V. Horvat, N. Nica, B. T. Roeder, E. McCleskey, R. E. Tribble and I. S. Towner, Phys. Rev. C **92**, 015502 (2015).
[11] R. G. Helmer, J. C. Hardy, V. E. Iacob, M. Sanchez-Vega, R. G. Neilson, and J. Nelson, Nucl. Instr. and Meth. in Phys. Res. A **511**, 360 (2003).
[12] R. G. Helmer, N. Nica, J. C. Hardy, and V. E. Iacob, Appl. Radiat. Isot. **60**, 173 (2004).
[13] E. Schönfeld, H Janssen, R. Klein, J. C. Hardy, V. Iacob, M. Sanchez-Vega, H. C. Griffin and M. A. Ludington, Appl. Radiat. Isot. **56**, 215 (2002).
[14] J. A. Halbleib, R. P. Kemsek, T. A. Mehlhorn, G. D. Valdez, S. M. Seltzer and M. J. Berger, Report SAND91-16734, Sandia National Labs (1992).
[15] S. Agostinelli *et al.*, Nucl. Instr. and Meth. in Phys. Res. A **506**, 250 (2003).
[16] V. V. Golovko, V. E. Iacob, and J. C. Hardy, Nucl. Instr. Meth. in Phys. Res. A **594**, 266 (2008).
[17] I. Kawrakow, Med. Phys. **27**, 485 (2000); I. Kawrakow and D. W. O. Rogers, NRCC Report PIRS-701, NRC, Ottawa (2003); https://nrc-cnrc.github.io/EGSnrc/.
[18] V. E. Iacob, J. C. Hardy, H. I. Park, M. Bencomo, L. Chen, V. Horvat, N. Nica, B. T. Roeder and A. Saastamoinen, Phys. Rev. C **101**, 015504 (2020).
[19] D. C. Radford, https://radware.phy.ornl.gov/main.html and private communication.
[20] J. C. Hardy, H. Schmeing, J. S. Geiger and R. L. Graham, Nucl. Phys. A **223**, 157 (1974).
[21] P. M. Endt, Nucl. Phys. A **521**, 1 (1990).
[22] P. M. DeLuca, J. C. Lawson, E. D. Berners and P. R. Chagnon, Nucl. Phys. A **173**, 307 (1971).
[23] H. I. Park *et al.*, in preparation.
[24] National Nuclear Data Center we site: www.nndc.bnl.gov.
[25] B. Singh, J. L. Rodriguez, S. S. M. Wong and J. K, Tuli, Nuclear Data Sheets **84**, 487 (1998).
[26] J. C. Hardy, L. C. Carraz, B. Jonson and P. G. Hansen, Phys. Lett. B **72**, 307 (1977).
[27] J. C. Hardy and I. S. Towner, Phys. Rev. Lett. **88**, 252501 (2002).
[28] B. H. Wildenthal, Prog. Part. Nucl. Phys. **11**, 5 (1984).
[29] B. A. Brown and W. A. Richter, Phys. Rev. C **74**, 034315 (2006).
[30] B. A. Brown and B. H. Wildenthal, At. Data and Nucl. Data Tables **33**, 347 (1985).